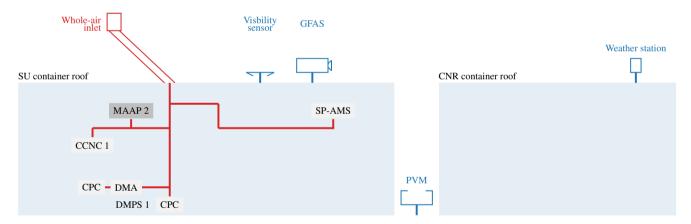# Supplementary material (SI) for "Importance of hydrated aerosol particles for aerosol-fog relationships in the Italian Po Valley"

Almuth Neuberger[1,2], Rahul Ranjan[1,2], Hao Ding[3,2], Fredrik Mattsson[1,2], Lea Haberstock[1,2], Darrel Baumgardner[4], Stefano Decesari[5], Annica M. L. Ekman[3,2], Dagen D. Hughes[4], Claudia Mohr[1,2,6,7], Marco Paglione[5], Ilona Riipinen[1,2], Matteo Rinaldi[5], and Paul Zieger[1,2]

[1]Department of Environmental Science, Stockholm University, Stockholm, Sweden
[2]Bolin Centre for Climate Research, Stockholm, Sweden
[3]Department of Meteorology, Stockholm University, Stockholm, Sweden
[4]Droplet Measurement Technologies, LLC, Longmont, USA
[5]Institute of Atmospheric Science and Climate, National Research Council of Italy, Bologna, Italy
[6]now at: Center for Energy and Environmental Sciences, Paul Scherrer Institute, Villigen, Switzerland
[7]now at: Department of Environmental Systems Science, ETH Zurich, Zurich, Switzerland

Correspondence: Paul Zieger (paul.zieger@aces.su.se)

The supplementary material is structured following the order of appearance in the main manuscript. First, more details on the methods, including the Large Eddy Simulation (LES) model evaluation, are given; afterwards, supporting material for the results.

Figure S1. Schematic of the experimental setup used for this study during Fog and Aerosol InteRAction Research Italy (FAIRARI) (adapted from Neuberger et al., 2025). Instruments behind a drier are indicated by a light gray background. Inlets/tubings of ambient air are colored. Ambient measurements are in blue. A list of acronyms can be found at the end of the main manuscript.

Table S1. Densities (ρ_i) and hygroscopicity parameters (κ_i) and the respective references of the assumed dry particle constituents.

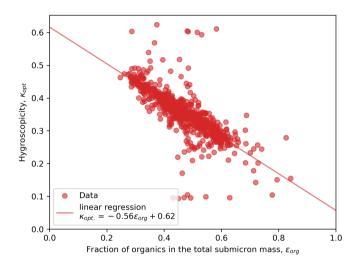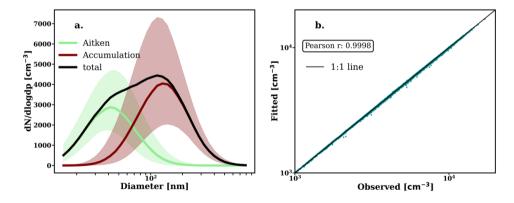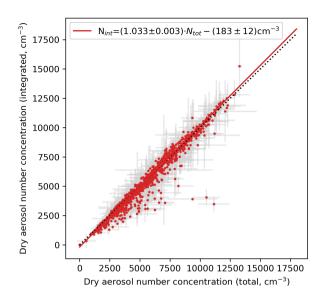| Compound	ρ (kg m^{-3})		κ	
Organics	1500	(Kostenidou et al., 2007)	0.10	(Fig. S2, Gunthe et al., 2009; Dusek et al., 2010)
Ammonium nitrate	1720	(Jurányi et al., 2010)	0.67	(Petters and Kreidenweis, 2007)
Ammonium sulfate	1769	(Jurányi et al., 2010)	0.61	(Petters and Kreidenweis, 2007)
Black Carbon	1770	(Jurányi et al., 2010)	0	(Weingartner et al., 1997)

Figure S2. Hygroscopicity parameter $\kappa_{opt.}$ vs. the organic fraction measured out of fog during FAIRARI. The red lines denotes a least-squared linear regression.

Figure S3. Separation of particle number size distribution into an Aitken and an accumulation mode. (a) median number size distributions for the Aitken (light green) and accumulation modes, as well as the total distribution (black line). The shaded regions represent the interquartile range (25th–75th percentiles) for both modes. The log-normal size distributions were calculated from the fit parameters obtained after applying the algorithm by Hussein et al. (2005) on observed size distributions. (b) Scatter plot of the total particle concentration from fitting versus the total particle concentration from observation with a 1:1 line (black).

Figure S4. Closure between the dry aerosol number concentration measured by the total Condensation Particle Counter (CPC) and the integrated size distribution. Mean values of 1 h are shown with the standard deviations shown as gray bars. The weighted bivariate linear fits were calculated following York et al. (2004).

Visibility calculation using Mie theory

Using the wet size distribution measured by the Ground-based Fog and Aerosol Spectrometer (GFAS), we calculated the visibility, applying Mie theory, χ_{Mie}. For that, the Koschmieder equation $\chi(\lambda) = 3.912/b_{\text{e}}(\lambda)$ (Koschmieder, 1924) has been adapted to the calibration of the here used visibility sensor, leading to a different numerator:

$$\chi_{\text{m}}(\lambda) = \frac{3}{b_{\text{e}}(\lambda)}. \tag{1}$$

The light extinction coefficient $b_{\text{e}}(\lambda)$ is composed of the light extinction coefficient from particles, $b_{\text{e,p}}(\lambda)$, and from Rayleigh scattering, $b_{\text{e,Rayleigh}}(\lambda)$ (ignoring further light extinction from trace gases):

$$b_{\text{e}}(\lambda) = b_{\text{e,p}}(\lambda) + b_{\text{e,Rayleigh}}(\lambda) = \int_{D_{\text{wet,min}}}^{D_{\text{wet,max}}} \pi \left(\frac{D_{\text{wet}}}{2} \right)^2 Q_{\text{e}}(\lambda, D_{\text{wet}}) \frac{\text{d}N_{\text{wet}}(D_{\text{wet}})}{\text{dlog} D_{\text{wet}}} \text{dlog} D_{\text{wet}} + b_{\text{e,Rayleigh}}(\lambda). \tag{2}$$

$Q_{\text{e}}(\lambda, D_{\text{wet}})$ is derived with the python module miepython at $\lambda = 880\,\text{nm}$ (the wavelength at which our visibility sensor measures). The refractive index of water is calculated to be about 1.327 at $\lambda = 880\,\text{nm}$, following Daimon and Masumura (2007).
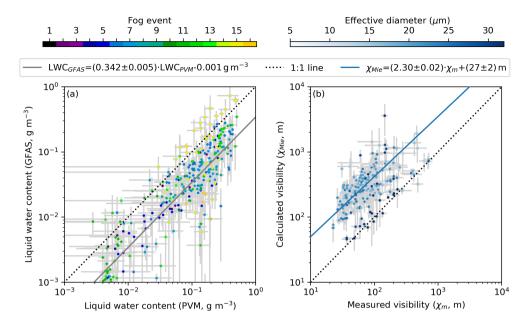
Figure S5. (a) Comparison of the liquid water content measurements by the Ground-based Fog and Aerosol Spectrometer (GFAS) and the Particle Volume Monitor (PVM) based on 10 min averages. The spearman correlation is 0.82, $p \ll 0.01$. (b) Measured vs. calculated visibility using Mie theory and the GFAS observations. The weighted bivariate linear fits were calculated following York et al. (2004).

Model evaluation

15   The baseline simulation for fog event 7 (i.e., case m7s7c7) was used to qualitatively evaluate the model performance from three aspects: the spatial development of the fog layer, the fog lifecycle, and microphysical properties within the fog. MIMICA captured key and typical features of the radiation fog, including the formation and the geometric thickening of the fog layer under longwave radiation cooling, as indicated by fog top lifting (Fig. S6). The simulated near-surface supersaturation is in reasonable agreement with that retrieved from observations (Fig. 4f). The model also represented the transition of strong radia-

20   tive cooling (or high-supersaturation areas) from the surface towards the fog top, indicating growing optical thickness. While the simulated fog formation, determined by a liquid water mixing ratio threshold of $0.01\,\text{g}\,\text{kg}^{-1}$, occurred nearly one hour later than the observed fog formation time based on visibility (Fig. 11). A possible reason for this discrepancy is the underestimation of the initial surface temperature and cooling rate, as the model surface forcing was based on 3.5 m observations, while actual surface temperatures in a stable boundary layer are typically lower. Despite this, the model captured the timing of fog

25   dissipation reasonably well.

Building on the microphysical evaluation, we examined the aerosol and droplet size distributions, along with the corresponding liquid water content (LWC) spectrum, averaged over the final four hours of event 7 (Fig. S7). MIMICA effectively represented the hygroscopic growth of dry aerosols and the key contribution of hydrated particles to the small-droplet fraction in droplet size distribution. The model also reproduced one peak of the droplet spectrum and its corresponding diameter.

30   Correspondingly, in the LWC spectrum, the distribution among small droplets ($D_{wet} < 25\,\mu m$) was well simulated, though the overestimation in the large droplets ($D_{wet} > 25\,\mu m$) was likely the primary cause of the overall high bias in total liquid water mixing ratio.
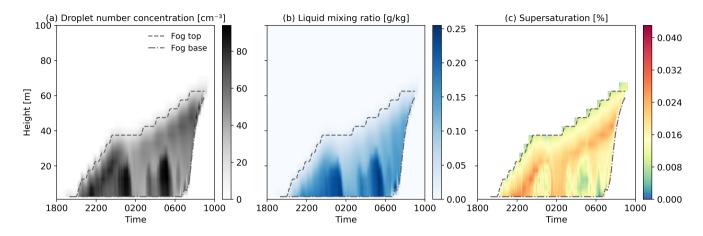

Figure S6. Vertical cross-sections of (a) droplet number concentration, (b) liquid water mixing ratio, and (c) supersaturation from simulations for the fog event on 18 -– 19 February 2022. The dashed lines indicate the fog base and top, defined as the height range where the droplet number concentration is $\geq 1\,cm^{-3}$ and the liquid water mixing ratio is $\geq 0.01\,g\,kg^{-1}$.
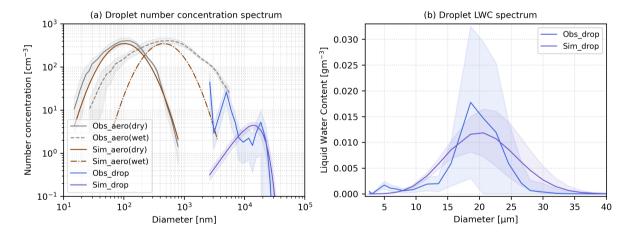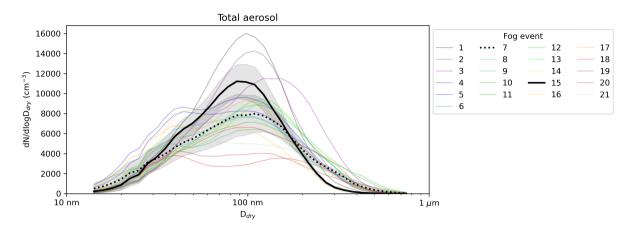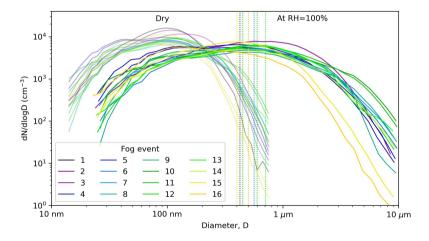

Figure S7. Mean size distributions of (a) aerosol and cloud droplet number concentrations and (b) droplet LWC from observations (obs) and simulations (sim), averaged over the last 4 hours of fog event 7. "Dry" and "wet" refer to aerosol states before and after hygroscopic growth, respectively. Shaded areas indicate ± 1 standard deviation.

Supporting material for main results

Figure S8. Mean dry particle number size distributions for the 21 fog events measured during FAIRARI. The two example fog events are highlighted in black with their standard deviation shaded in gray.

Figure S9. Median size distributions (dry and at 100 % relative humidity) for the fog events measured during FAIRARI. The median dry activation diameters are shown as vertical lines.

Using the LES model MIMICA, we analyzed the sensitivity of fog microphysics to the physicochemical properties of aerosol particles. The study employed identical meteorological conditions corresponding to event 7 (m7), while systematically varying combinations of aerosol size (s7, s15) and composition (c7, c15) properties from events 7 and 15 (Fig. S10), resulting in four distinct simulation scenarios: m7s7c7, m7s7c15, m7s15c7, and m7s15c15.
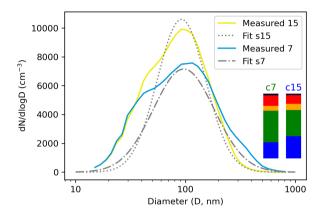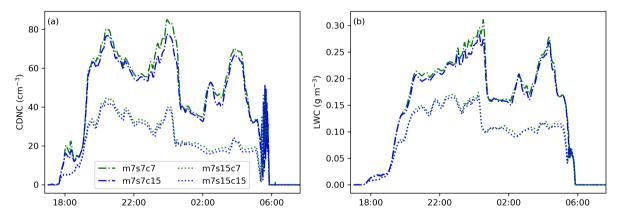

Figure S10. Input parameters for LES modeling. Measured dry aerosol number size distribution (together with a single lognormal fit) and chemical composition for fog event 7 and 15.

Figure S11. Sensitivity of LES code MIMICA to physicochemical aerosol properties. (a) cloud droplet number concentration (CDNC), (b) liquid water content (LWC) for different combinations of the dry aerosol number size distribution and κ, using the meteorology of fog event 7, as described in Fig. S10.
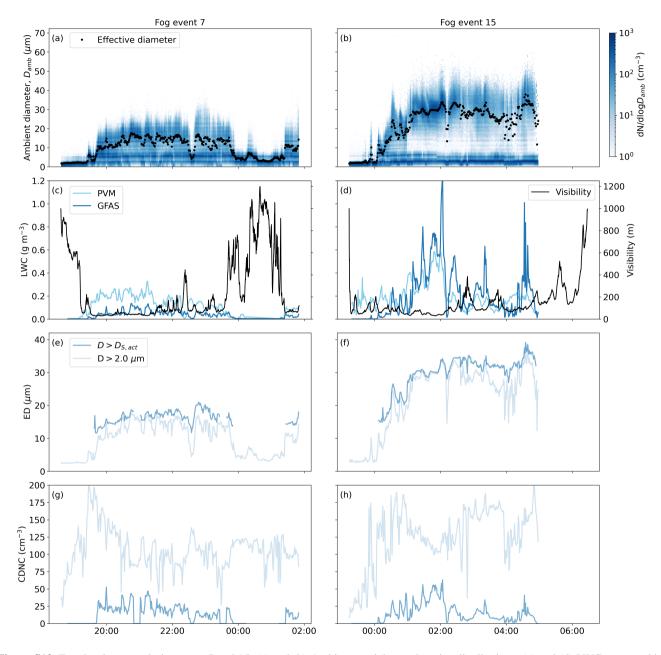
Figure S12. Fog development during event 7 and 15. (a) and (b) Ambient particle number size distributions. (c) and (d) LWC measured by the GFAS (darkblue) and the Particle Volume Monitor (PVM) (lightblue) and measured visibility. effective diameter (ED) and cloud droplet number concentration (CDNC) are calculated with two different lower diameters ($D_{wet} > 2\,\mu$m and D_{wet,act_S}) in (e)−(h).
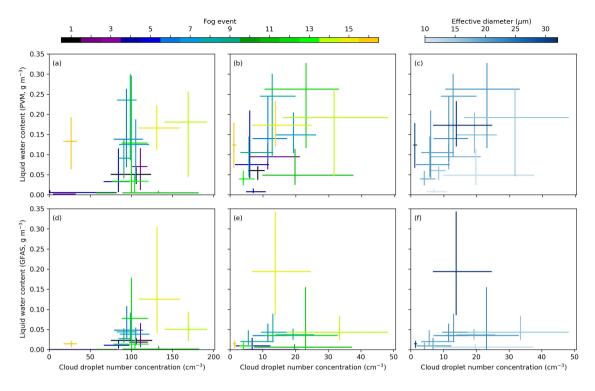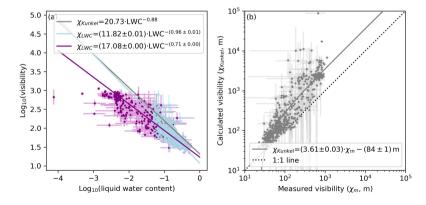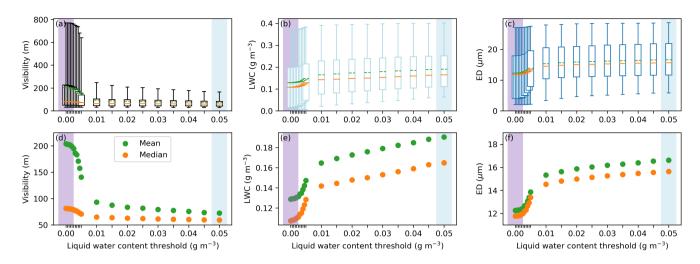
Figure S13. Effect of hydrated aerosol particles on cloud droplet number concentration (CDNC). The interquartile ranges are shown for each fog event. (a) and (d) CDNC is calculated for $D_{wet} > 2\,\mu$m. (b) and (e) CDNC is calculated for $D_{wet} > D_{wet,act\_S}$. (c) and (f) as (b) and (e) but colorcoded by the median ED. (a)–(c) Liquid water content as measured by the PVM, (d)–(f) liquid water content as measured by the GFAS. Only times were both instruments were measuring are included. The peak seen in Fig. 6(b) at CDNC $= 0\,\text{cm}^{-3}$ is excluded.

Figure S14. Visibility derived from LWC measurements with and without hydrated aerosol particles. (a) 10 min averages are shown for the visibility-only definition of fog (purple) and an additional liquid water content (LWC) threshold of $0.05\,\text{g}\,\text{m}^{-3}$ (lightblue). The visibility is calculated with a bivariate linear fit (following York et al., 2004) on the logarithm of the LWC. The parameterization by Kunkel (1984) is shown as gray line for comparison. (b) Derived visibility vs. measured visibility using the parameterization by Kunkel (1984).

Figure S15. Effect of different fog definitions on fog microphysical parameters. In addition to the visibility criteria, a liquid water content threshold is added and varied between 0 and 0.1 g m^{-3} to define a fog event. (a) and (d) Effect on visibility range, (b) and (e) effect on liquid water content, and (c) and (f) effect on effective diameter. In the upper panel, the boxes represent the 25 and 75 percentiles and the whiskers the 5 and 95 percentiles. The mean is given in green, the median in orange.
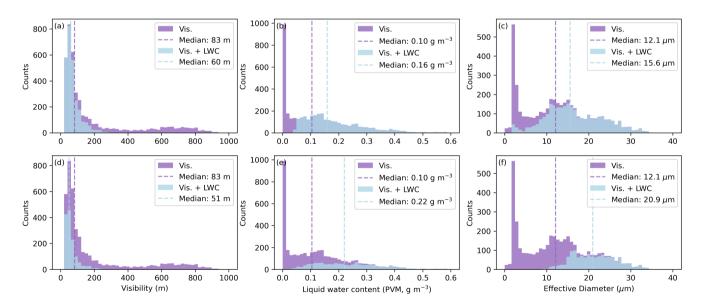

Figure S16. Effect of three different fog definitions applied on fog statistics for two different instruments. The commonly used fog definition (vis. $<$ 1 km, purple) is compared to the combined definition (vis. $<$ 1 km + LWC $>$ 0.05 g m^{-3}, light blue). (a) $-$ (c) Liquid water content threshold as measured by the PVM, (d) $-$ (f) liquid water content threshold as measured by the GFAS. Only times were both instruments were measuring are included.
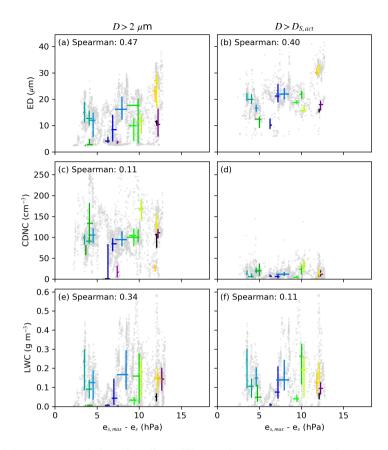
Figure S17. Campaign-based Spearman correlation of cooling (difference between water saturation vapor pressure corresponding to the maximum temperature of the day and that to the current temperature) and fog microphysical parameters. (a) and (b) correlation with the effective diameter (ED). (c) and (d) correlation with the cloud droplet number concentration (CDNC). (e) and (f) correlation with the liquid water content (LWC). (a), (c), and (e) for $D_{wet} > 2\,\mu$m, (b), (d), and (f) for $D_{wet} > D_{wet,act\_S}$. The interquartile ranges of the fog events are shown, color-coded by the number of the fog events. The Spearman correlation is based on all underlying data points (grey dots) and given if $p < 0.01$. The LWC is taken from the PVM measurements. The data is based on 1 min averages.

References

Daimon, M. and Masumura, A.: Measurement of the refractive index of distilled water from the near-infrared region to the ultraviolet region, Appl. Opt., 46, 3811–3820, https://doi.org/10.1364/AO.46.003811, 2007.

Dusek, U., Frank, G. P., Curtius, J., Drewnick, F., Schneider, J., Kürten, A., Rose, D., Andreae, M. O., Borrmann, S., and Pöschl, U.: Enhanced organic mass fraction and decreased hygroscopicity of cloud condensation nuclei (CCN) during new particle formation events, Geophysical Research Letters, 37, https://doi.org/https://doi.org/10.1029/2009GL040930, 2010.

Gunthe, S. S., King, S. M., Rose, D., Chen, Q., Roldin, P., Farmer, D. K., Jimenez, J. L., Artaxo, P., Andreae, M. O., Martin, S. T., and Pöschl, U.: Cloud condensation nuclei in pristine tropical rainforest air of Amazonia: size-resolved measurements and modeling of atmospheric aerosol composition and CCN activity, Atmospheric Chemistry and Physics, 9, 7551–7575, https://doi.org/10.5194/acp-9-7551-2009, 2009.

Hussein, T., Dal Maso, M., Petäjä, T., Koponen, I. K., Paatero, P., Aalto, P. P., Hämeri, K., and Kulmala, M.: Evaluation of an automatic algorithm for fitting the particle number size distributions, Boreal environment research, 10, 337, 2005.

Jurányi, Z., Gysel, M., Weingartner, E., DeCarlo, P. F., Kammermann, L., and Baltensperger, U.: Measured and modelled cloud condensation nuclei number concentration at the high alpine site Jungfraujoch, Atmospheric Chemistry and Physics, 10, 7891–7906, https://doi.org/10.5194/acp-10-7891-2010, 2010.

Koschmieder, H.: Theorie der horizontalen sichtweite, Beitrage zur Physik der Freien Atmosphare, Meteorologische Zeitschrift, 12, 3353, 1924.

Kostenidou, E., Pathak, R., and Pandis, S.: An Algorithm for the Calculation of Secondary Organic Aerosol Density Combining AMS and SMPS Data, Aerosol Science and Technology, 41, 1002–1010, https://doi.org/10.1080/02786820701666270, 2007.

Kunkel, B. A.: Parameterization of Droplet Terminal Velocity and Extinction Coefficient in Fog Models, Journal of Applied Meteorology and Climatology, 23, 34 – 41, https://doi.org/10.1175/1520-0450(1984)023<0034:PODTVA>2.0.CO;2, 1984.

Neuberger, A., Decesari, S., Aktypis, A., Andersen, H., Baumgardner, D., Bianchi, F., Busetto, M., Cai, J., Cermak, J., Dipu, S., Ekman, A., Fuzzi, S., Gramlich, Y., Haslett, S. L., Heikkinen, L., Joutsensaari, J., Kaltsonoudis, C., Kangasluoma, J., Krejci, R., Lupi, A., Marinoni, A., Matrali, A., Mattsson, F., Mohr, C., Nenes, A., Paglione, M., Pandis, S. N., Patel, A., Riipinen, I., Rinaldi, M., Steimer, S. S., Stolzenburg, D., Sulo, J., Vasilakopoulou, C. N., and Zieger, P.: From Molecules to Droplets: The Fog and Aerosol Interaction Research Italy (FAIRARI) 2021/22 Campaign, Bulletin of the American Meteorological Society, 106, E23 – E50, https://doi.org/10.1175/BAMS-D-23-0166.1, 2025.

Petters, M. D. and Kreidenweis, S. M.: A single parameter representation of hygroscopic growth and cloud condensation nucleus activity, Atmospheric Chemistry and Physics, 7, 1961–1971, https://doi.org/10.5194/acp-7-1961-2007, 2007.

Weingartner, E., Burtscher, H., and Baltensperger, U.: Hygroscopic properties of carbon and diesel soot particles, Atmospheric Environment, 31, 2311–2327, https://doi.org/https://doi.org/10.1016/S1352-2310(97)00023-X, 1997.

York, D., Evensen, N. M., Martı́nez, M. L., and De Basabe Delgado, J.: Unified equations for the slope, intercept, and standard errors of the best straight line, American journal of physics, 72, 367–375, 2004.